AIAA SciTech Forum
23-27 January 2023, National Harbor, MD & Online
AIAA SCITECH 2023 Forum

10.2514/6.2023-1466

Adaptive Modeling of Supersonic Combustion in a Cavity-Stabilized Scramjet

Matthew Bonanni*, Andrew Norris†, and Matthias Ihme‡
Stanford University, Stanford, CA, 94305

Large-eddy simulations of scramjet engines with accurate combustion modeling is generally prohibitively expensive because of the complex combustion processes occurring within these systems. Under these conditions, traditional tabulated chemistry methods perform poorly, leading to a reliance on finite-rate chemistry. The Pareto-efficient combustion (PEC) framework enables the dynamic assignment of different combustion models to specific regions of the computational domain, based on user-specified accuracy of quantities of interest and cost requirements. This enables the simulation to maintain fidelity where necessary and otherwise reduce cost where possible. To date, this framework has only been applied to low-Mach combustion problems. This work extends this PEC framework to supersonic combustion via application to steady-state combustion in the RC19 scramjet combustor rig at Wright-Patterson Air Force Base. The effectiveness of the framework is demonstrated via a comparison against experimental data to evaluate simulation accuracy.

I. Nomenclature

ρ	=	density
$\mathbf{u}$	=	velocity vector
p	=	pressure
τ	=	stress
E	=	total energy
$\mathbf{q}$	=	heat flux vector
$\boldsymbol{\phi}$	=	chemical state vector
$\mathbf{j}$	=	chemical flux vector
$\mathbf{S}_\phi$	=	source vector of chemical state
$\mathcal{M}$	=	submodel mapping
Ω	=	computational domain
M	=	set of candidate combustion submodels
e	=	submodel error
c	=	submodel cost
λ	=	PEC cost penalty parameter
ψ	=	quantity of interest
$\mathcal{D}$	=	drift term

II. Introduction

Large-eddy simulation has been widely used for simulations of subsonic combustion in systems such as gas-turbine combustors and rocket engines, but scramjet simulations are often prohibitively expensive. This is due in large part to the difficulty in simulating the complex thermochemical processes of supersonic combustion. Under these conditions, significant pressure variations, flame/wall coupling, and unsteady effects such as ignition and shock/flame coupling render low-dimensional manifold models such as flamelet models insufficient for this application as currently formulated. Additionally, even in subsonic conditions, the low computational cost of tabulated chemistry models comes at the

*PhD Candidate, Department of Mechanical Engineering, 440 Escondido Mall, Stanford, CA 94305, AIAA Student Member.
†Assistant Branch Head for Hypersonic Air-Breathing Propulsion, NASA Langley Research Center, 1 NASA Dr, Hampton, VA 23666.
‡Professor of Mechanical Engineering and of Photon Science, Department of Mechanical Engineering, 440 Escondido Mall, Stanford, CA 94305.

expense of fidelity, especially when predicting minor species [1]. In contrast, finite-rate chemistry (FRC) approaches offer improved fidelity, but their cost is often prohibitive, especially for large hydrocarbon fuels.

To address this issue, the Pareto-efficient combustion (PEC) framework of Wu et al. [1] dynamically and locally assigns combustion submodels across the computational domain. The user specifies a set of candidate combustion submodels, a weight coefficient λ which balances cost and accuracy, and a set of quantities of interest (QoIs) whose error is to be minimized. The choice of these QoIs enables simulations to be tailored to specific applications, including the prediction of CO emissions, ignition, and spray combustion [2, 3]. In practical low-Mach applications such as turbulent jet flames, the PEC framework has been demonstrated to significantly improve CO prediction compared to flamelet models by applying FRC to only 9% of the domain, at less than half the cost of a full FRC simulation [4]. The present work extends the PEC framework to supersonic combustion in the context of a scramjet engine, in order to reduce the computational expense while retaining simulation accuracy.

III. Computational Approach

The large-eddy simulation presented in this work numerically solves the fully-compressible Navier-Stokes equations, considering the Favre-filtered conservation laws of mass, momentum, energy, and chemical species:

$$\partial_t \overline{\rho} + \nabla \cdot (\overline{\rho}\widetilde{\mathbf{u}}) = 0, \tag{1}$$

$$\partial_t \left(\overline{\rho}\widetilde{\mathbf{u}}\right) + \nabla \cdot \left(\overline{\rho}\widetilde{\mathbf{u}}\widetilde{\mathbf{u}} + \overline{p}\mathbf{I}\right) = \nabla \cdot \left(\overline{\tau} + \tau_{\text{sgs}}\right), \tag{2}$$

$$\partial_t \left(\overline{\rho}\widetilde{E}\right) + \nabla \cdot \left(\overline{\rho}\widetilde{E}\widetilde{\mathbf{u}} + \overline{p}\right) = \nabla \cdot \left[\left(\overline{\tau} + \tau_{\text{sgs}}\right) \cdot \widetilde{\mathbf{u}} - \left(\overline{\mathbf{q}} + \mathbf{q}_{\text{sgs}}\right)\right], \tag{3}$$

$$\partial_t \left(\overline{\rho}\widetilde{\boldsymbol{\phi}}\right) + \nabla \cdot \left(\overline{\rho}\widetilde{\mathbf{u}}\widetilde{\boldsymbol{\phi}}\right) = -\nabla \cdot \left(\overline{\mathbf{j}} + \mathbf{j}_{\text{sgs}}\right) + \overline{\mathbf{S}}_{\phi}, \tag{4}$$

where ρ is the density $\mathbf{u}$ is the velocity vector, p is the pressure, τ is the stress tensor, E is the total energy, and $\mathbf{q}$ is the heat flux. $\boldsymbol{\phi}$ is the vector of manifold-describing variables of all candidate models, with corresponding flux vector $\mathbf{j}$ and chemical source term $\mathbf{S}_{\phi}$.

The submodel assignment, represented by the mapping $\mathcal{M} : \Omega \rightarrow M$, where $\mathcal{M}$ is the map of assigned submodels, Ω is the computational domain, and M is the set of candidate submodels. A detailed description of the PEC framework is presented in [1]. PEC determines this assignment by minimizing the weighted sum of the estimated error and cost:

$$\min_{\mathcal{M}:\Omega\rightarrow M} \left(\int_{\Omega} e\left(M\left(\mathbf{x}\right), \mathbf{x}\right) d\mathbf{x} + \lambda \int_{\Omega} c\left(M\left(\mathbf{x}\right), \mathbf{x}\right) d\mathbf{x} \right) \tag{5}$$

where the penalty parameter λ adjusts the weighting by penalizing cost. Higher values of λ result in model assignment which yields lower cost and higher error. The cost, c, is constant for a given model and evaluated as its number of transported scalars, because the numerical formulation scales approximately linearly with this quantity [1].

The error, e, represents the local difference between the true state $\boldsymbol{\phi}$ and the modeled state $\hat{\boldsymbol{\phi}}$ for a particular submodel. In order to avoid the need for knowledge of the true state, which would require a detailed simulation thus negating the benefits of the dynamic submodel assignment, the drift term of QoI ψ and model m, $\widetilde{\mathcal{D}}_{\psi}^{m}$, is computed for a particular set of QoIs, $Q = \left\{\widetilde{\psi}_1, \ldots, \widetilde{\psi}_{N_Q}\right\}$:

$$\widetilde{\mathcal{D}}_{\psi}^{m} = \overline{\rho}\widetilde{D}_t\widetilde{\psi}|_{\widetilde{\psi}=\widetilde{\psi}^m} - \overline{\rho}\frac{\partial\widetilde{\psi}^m}{\partial\widetilde{\boldsymbol{\phi}}^m} \cdot \widetilde{D}_t\widetilde{\boldsymbol{\phi}}^m, \tag{6}$$

where $\widetilde{\psi}^m$ is the QoI evaluated using the solution of model m. This drift term describes the growth rate of the manifold error, where the first term represents the material derivative of the QoI based on the current state of the flow field, and the second term is the material derivative of the QoI as predicted by the manifold variables of model m, $\widetilde{\boldsymbol{\phi}}^m$.

These equations are solved using an unstructured finite volume solver [5, 6]. This solver uses a sensor-based hybrid scheme to compute the Euler fluxes, and a nominally fourth-order scheme for the viscous fluxes. A simple balancing splitting scheme is used for time-stepping, with a fourth-order semi-implicit Rosenbrock-Krylov scheme being used for the stiff reaction terms of the FRC submodel while a third-order strong stability preserving Runge-Kutta scheme is used for the non-stiff terms [7]. A shock sensor based on density gradients is applied to avoid numerical instability, with a 2nd order essentially-non-oscillatory scheme being used in these regions. ODE-based, isothermal wall models are used at each of the walls of the domain.

The set of candidate models for the PEC framework includes an FRC model based on the 14-species skeletal ethylene-air mechanism of Gokulakrishnan et al. [8], a flamelet-progress variable (FPV) model using tabulated chemistry computed from this mechanism [9], and an inert mixing model.

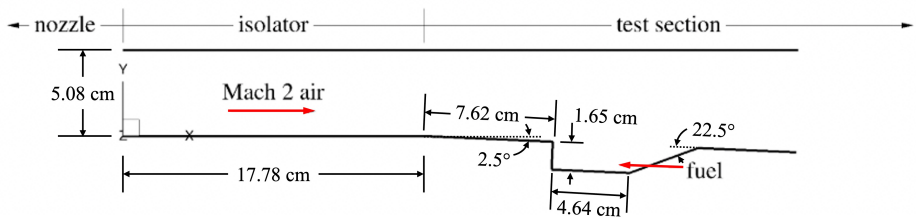

Fig. 1 Schematic of the model scramjet combustor at the RC19 facility, WPAFB, adapted from [11].

IV. Experimental Configuration

The present work simulates the supersonic combustion experiments performed in Research Cell 19 at Wright-Patterson Air Force Base [10]. This facility is configured with an ethylene-fueled model scramjet combustor with a cavity flameholder configuration, depicted in fig. 1. While various fuel injection strategies are used [12], the present work considers the most commonly-used configuration of eleven spanwise injectors in the cavity ramp region [13, 14]. The inlet air is supplied by a Mach 2.0 facility nozzle [10].

V. Computational Configuration

A. Domain

As in the work of [11], a spanwise periodic section of the combustor was isolated for this simulation, containing two of the eleven injectors (one injector is split by the periodic plane). Upstream, the domain begins at the point where the bottom wall of the combustor begins to ramp downwards, and the domain continues downstream approximately 5 cm past the lip of the cavity ramp. This domain was chosen to reduce the computational cost while capturing the necessary combustion physics. The plenum upstream of the fuel injectors was not modeled; instead each injector was extended to a length $L = 1.5$ cm for $L/D \geq 5$.

A structured mesh with 5.0 million cells was developed for this domain. This mesh has a minimum grid spacing of 50 μm at the walls, corresponding to a y^+ value of 50, suitable for the wall model employed here.

B. Conditions

To enable comparisons to the widest array of available experimental data, the simulation here is performed at Mach 2 conditions. The stagnation temperature and pressure of the incoming airflow are 589 K and 483 kPa, respectively. Ethylene fuel is injected through the two injectors of this section at a mass flux consistent with the 56 SLPM fueling case in the full combustor. A subsonic mass flux-enforcing boundary condition was used for these injectors, and the mass flux was verified *a posteriori*. The air inflow is also injected with turbulence and a boundary layer profile derived from hybrid RANS-LES simulations performed by Peterson et al. [11].

With the exception of the front and rear walls, which are periodic, all walls in this simulation are treated as isothermal at a temperature of 300 K, and a supersonic boundary condition is applied at the outlet. For cell-faces at the outlet boundary for which the velocity is subsonic, such as in the boundary layers, an outlet pressure lower than the cell pressure is specified in order to prevent reversed flow.

For the PEC combustion framework, four QoIs are considered, corresponding to the constitutive species of the progress variable: the mass fractions of CO, CO_2, H_2, and H_2O, each with equal weight. These have been selected because they are involved in the most significant exothermic reactions, thereby serving as a proxy for heat release. The drift term is computed for these species and the resulting error dictates the submodel assignment as described in Section III

VI. Results

Instantaneous and time-averaged contours of axial velocity, pressure, and temperature are presented in fig. 2. In the velocity contours, we note the presence of the shear layer and recirculation zone created by the cavity, creating a low-speed region in which the flame is stabilized. In the contours of pressure, an expansion fan is visible at the start of

the ramped section of the lower wall, and this fan is reflected off of the top wall of the chamber. Oblique shocks are also visible at the leading and trailing edges of the cavity, again reflecting off the top wall. Finally, in the temperature contours, we note the presence of a hot recirculation region in the upstream half of the cavity, reaching temperatures upwards of 2000 K. These hot combustion products are advected out of the cavity by the shear layer and are carried downstream towards the outlet.

In fig. 3, instantaneous and time-averaged mass fraction contours of OH are depicted in order to evaluate experimental agreement. Comparisons with the OH-PLIF imaging data from the RC19 experiment as depicted in Figure 2 of Hammack et al. [15] reveal good agreement in both the time-averaged and instantaneous profiles.

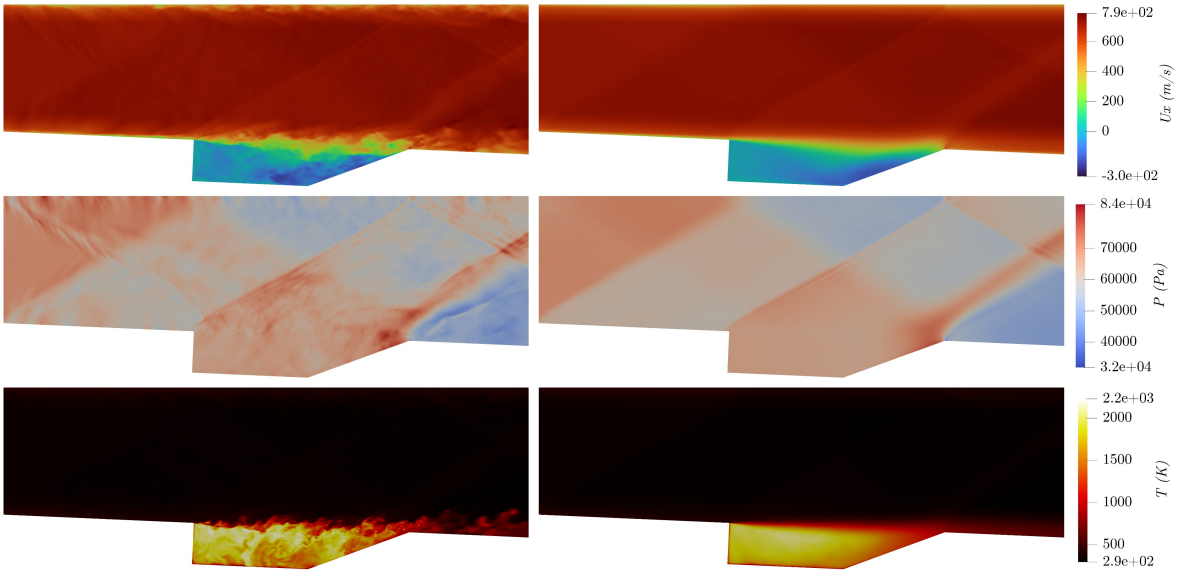

Fig. 2 Instantaneous (left) and time-averaged (right) contours of axial velocity (top), pressure (middle), and temperature (bottom) from large-eddy simulation of steady-state combustion in the RC19 scramjet combustor.

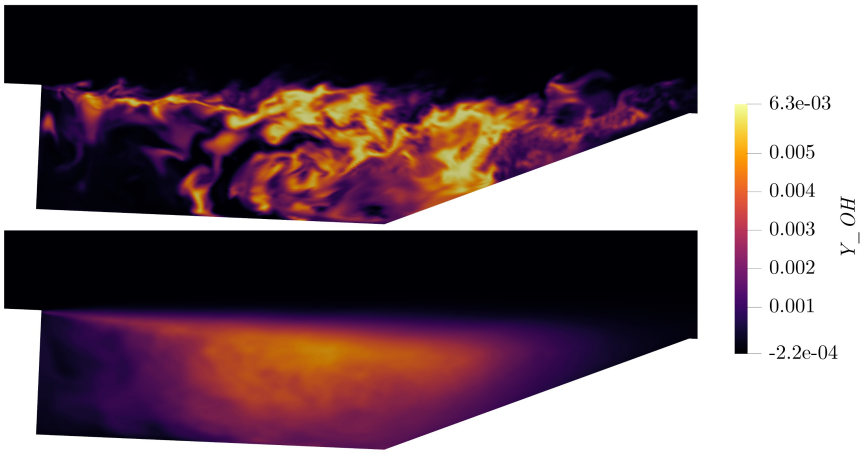

Fig. 3 Instantaneous (top) and time-averaged (bottom) OH mass fraction in the RC19 cavity.

Finally, in fig. 4, the submodel assignment is depicted. An instantaneous snapshot is presented in coordination with a time-averaged probability of FRC assignment. We note that the FRC submodel is applied to less than 11% of the domain, while FPV is applied everywhere else. Furthermore, FRC is localized in two primary locations: the turbulent shear layer and a bubble surrounding the point of injection. This aligns with intuitive expectations that these are the most complex and chemically active regions of the cavity combustor. These regions exhibit strong flame interaction

effects for which flamelet models are inadequate. The shear layer also exhibits significant pressure variation, leading to compressibility effects which standard flamelet models do not account for. We note that the application of FRC is also correlated with the heat release rate. In the shear layer, turbulent mixing entrains air into the cavity and combustion occurs in this well-mixed region. Inside the cavity, the highest heat release rates are again colocated with the application of FRC.

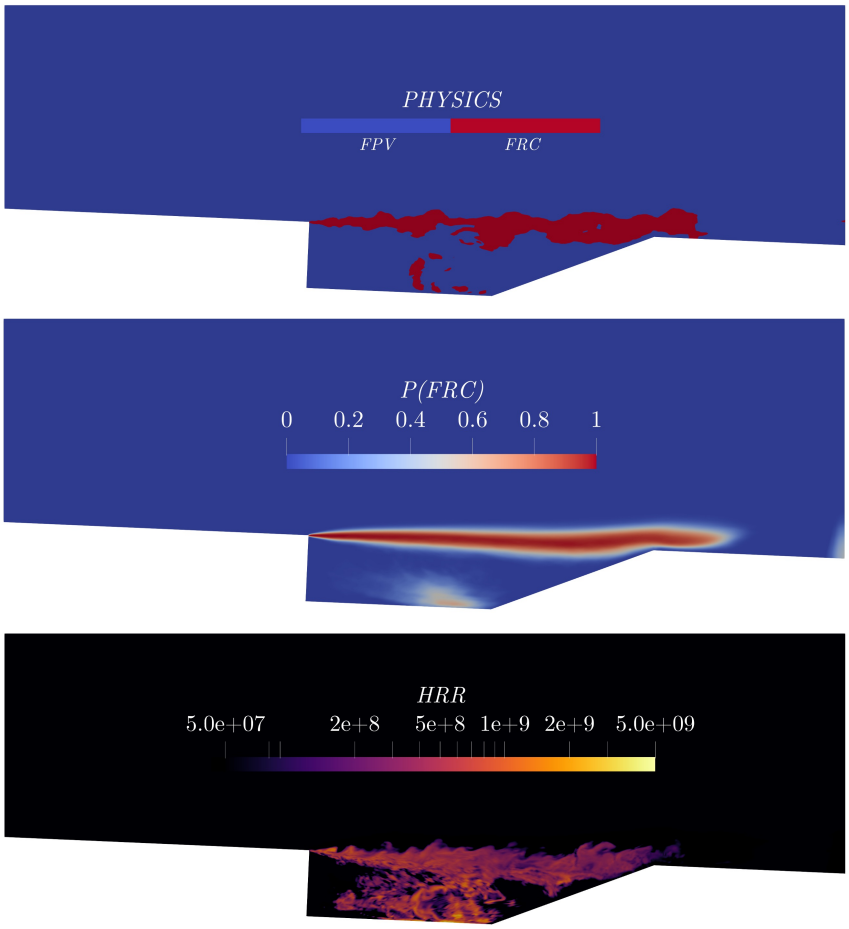

Fig. 4 Localized application of combustion models in the PEC framework, time-averaged probability of finite rate chemistry assignment, and comparison with the heat release rate.

VII. Conclusion

This study presents initial results assessing the feasibility of applying the PEC framework to high-speed combustion. With a preliminary selection of quantities of interest, we have demonstrated that the PEC framework with the drift term sensor-based submodel assignment successfully applies finite-rate chemistry modeling in regions exhibiting features for which flamelet models are known to be inadequate, such as the compressible shear layer. This application is additionally correlated with the heat release rate, indicating that the most significant exothermic reactions are being modeled with high fidelity. Finally, finite-rate chemistry is applied to less than 11% of the computational domain, eliminating the need for expensive integration of stiff chemical kinetic mechanisms in regions with low chemical activity.

Having demonstrated the feasibility of this approach, future work includes the selection of optimal quantities of interest which minimize the error in prediction of relevant global engineering quantities such as thrust and specific impulse. Furthermore, the introduction of flamelet models which account for compressibility effects may further reduce the error of the tabulated chemistry submodel, thereby reducing the assignment of finite-rate chemistry.

Acknowledgments

Financial support by the NASA Fellowship Activity program, training grant #80NSSC21K2054, is gratefully acknowledged. The authors also thank Drs. David Peterson, Timothy Ombrello, and Campbell Carter of the Air Force Research Laboratory for sharing the turbulent inflow data and for technical discussions.

References

[1] Wu, H., See, Y. C., Wang, Q., and Ihme, M., "A Pareto-efficient combustion framework with submodel assignment for predicting complex flame configurations," *Combust. Flame*, Vol. 162, No. 11, 2015, pp. 4208–4230.

[2] Douasbin, Q., Ihme, M., and Arndt, C., "Pareto-efficient combustion framework for predicting transient ignition dynamics in turbulent flames: Application to a pulsed jet-in-hot-coflow flame," *Combustion and Flame*, Vol. 223, 2021, pp. 153–165.

[3] D. Mohaddes, D. B., and Ihme, M., "Cost-constrained adaptive simulations of transient spray combustion in a gas turbine combustor," *Combustion and Flame*, 2023. In press.

[4] Wu, H., Ma, P. C., Jaravel, T., and Ihme, M., "Pareto-efficient combustion modeling for improved CO-emission prediction in LES of a piloted turbulent dimethyl ether jet flame," *Proc. Combust. Inst.*, Vol. 37, No. 2, 2019, pp. 2267–2276.

[5] Khalighi, Y., Nichols, J. W., Lele, S. K., Ham, F., and Moin, P., "Unstructured large eddy simulation for prediction of noise issued from turbulent jets in various configurations," *17th AIAA/CEAS Aeroacoustics Conf. 2011 (32nd AIAA Aeroacoustics Conf.*, 2011. https://doi.org/10.2514/6.2011-2886, URL http://arc.aiaa.org.

[6] Ma, P. C., Lv, Y., and Ihme, M., "An entropy-stable hybrid scheme for simulations of transcritical real-fluid flows," *J. Comput. Phys.*, Vol. 340, 2017, pp. 330–357.

[7] Wu, H., Ma, P. C., and Ihme, M., "Efficient time-stepping techniques for simulating turbulent reactive flows with stiff chemistry," *Comput. Phys. Commun.*, Vol. 243, 2019, pp. 81–96.

[8] Gokulakrishnan, P., Pal, S., Klassen, M., Hamer, A., Roby, R., Kozaka, O., and Menon, S., "Supersonic Combustion Simulation of Cavity-Stabilized Hydrocarbon Flames using Ethylene Reduced Kinetic Mechanism," *42nd AIAA/ASME/SAE/ASEE Joint Propulsion Conference & Exhibit*, Joint Propulsion Conferences, American Institute of Aeronautics and Astronautics, 2006. https://doi.org/10.2514/6.2006-5092, URL https://arc.aiaa.org/doi/10.2514/6.2006-5092.

[9] Ihme, M., Cha, C. M., and Pitsch, H., "Prediction of local extinction and re-ignition effects in non-premixed turbulent combustion using a flamelet/progress variable approach," *Proc. Combust. Inst.*, Vol. 30, 2005, pp. 793–800.

[10] Gruber, M. R., and Nejad, A. S., "New supersonic combustion research facility," *J. Propuls. Power*, Vol. 11, No. 5, 1995, pp. 1080–1083.

[11] Peterson, D. M., Hassan, E., Tuttle, S. G., Hagenmaier, M., and Carter, C. D., "Numerical investigation of a supersonic cavity flameholder," *AIAA SciTech Forum*, National Harbor, MD, 2014, AIAA-Paper 2014-1158.

[12] Gruber, M. R., Donbar, J. M., Carter, C. D., and Hsu, K.-Y., "Mixing and combustion studies using cavity-based flameholders in a supersonic flow," *J. Propuls. Power*, Vol. 20, No. 5, 2004, pp. 769–778.

[13] Ombrello, T., Hassan, E., Carter, C., McGann, B., Lee, T., Do, H., Peterson, D., Ivancic, P., and Luke, E., "Establishing the controlling parameters of ignition in high-speed flow," *AIAA SciTech Forum*, San Diego, CA, 2016, AIAA-Paper 2016-0658.

[14] Okhovat, S., Ombrello, T., and Resor, M. I., "Radiance of select species in a scramjet cavity," *AIAA SciTech Forum*, Grapevine, TX, 2017, AIAA-Paper 2017-0340.

[15] Hammack, S. D., Lee, T., Hsu, K. Y., and Carter, C. D., "High-repetition-rate OH planar laser-induced fluorescence of a cavity flameholder," *Journal of Propulsion and Power*, Vol. 29, No. 5, 2013, pp. 1248–1251. https://doi.org/10.2514/1.B34756.